Measurement of the Medial Plantar Arch using Shadow Moiré

Rodrigo Franco Corrêa da Costa
rodrigofcc@bol.com.br

Elaine Maria Ribeiro
elainemribeiro@hotmail.com

Meinhard Sesselmann, Dr.-Eng.
meinhard@ufmg.br

The purpose of this study is to perform profile measurements of human body parts using Shadow Moiré. The measurement results are used to assist medical personal in diagnosis and evaluation of patients. The system is composed only of low-cost standard optical components in order to turn it easily accessible for private offices. For automatic quantification of profiles the system combines Shadow Moiré with phase-shifting.

The object of study, here, was a plaster-cast of a foot. Four images were acquired in four different positions. Dedicated software was developed to process the images and to calculate the foot's profile automatically. In addition to that, a brief metrological analysis is presented in order to estimate the measurement uncertainty of the system. The estimated value was verified by direct comparison of the calculated profile with that obtained by a coordinate measurement machine.

Results obtained with this non-contact optical system demonstrate that combined uncertainties lower than 5%, relative to the measured value, are feasible. The principal advantages of this system, which are its simple set-up, the absence of contact and low cost, makes it a good choice for enhancing the reliability of profile measurements of human body parts and speeding up the process of diagnosis in private offices.

Key words: *Moiré, Shadow Moiré, 3D form measurement, Phase-Shifting*

1) INTRODUCTION

Hebert et al (2003) shows that the medial plantar arch is an extremely important area for the study of the posture, static and dynamic muscular balance of the human being's. Its dysfunction is the cause or consequence of several pathologies, painful pictures and functional disturbances. Andrews et al (2000), shows that several methods are used to evaluate and to study this area, among them the plantar impression of the patient for clinical evaluation, the so-called podograms, and imaging methods using X-rays. Hanra et al (1994) concludes that the uncertainty margin is relatively high for all those methods. Therefore, new measurement techniques are being tested that quantify, preferably without contact, the whole profile of the plantar arch of the foot with the intention to get simpler, faster and more reliable methods for diagnosis.

The Moiré method has been used for surface profiling in several areas for a long time. Takasaki (1970), was the first to use the Moiré method to profile human body parts. Gold et al were the first ones to analyze the plantar surface, however without information about uncertainties in their experiment. Recently, Volpon (1994) presented a method for quantitative evaluation. However, as in several other applications using Moiré, no analysis of error was made, which reduces the reliability of the presented results. Furthermore, the proposed method was far from measuring automatically, which is one of the preconditions to spread its usage outside the laboratory.

The goal of this work is to demonstrate the applicability of Shadow Moiré in combination with phase shifting to measure automatically the profile of the medial arch with uncertainties, sufficiently small for fast and safe diagnoses. The overall system should be simple to set up and contain only low cost standard optical components in order to be run by non-technical personal with minimum training.

2) THEORY

Figure 1 illustrates the usual arrangement of choice for Shadow Moiré (Gasvik 1995, Post et al 1989. If an object ***O*** is illuminated from a light source ***S*** through a grating ***G*** with pitch ***p*** closely in front of it, shadows of the grating lines will be projected upon the surface under study.

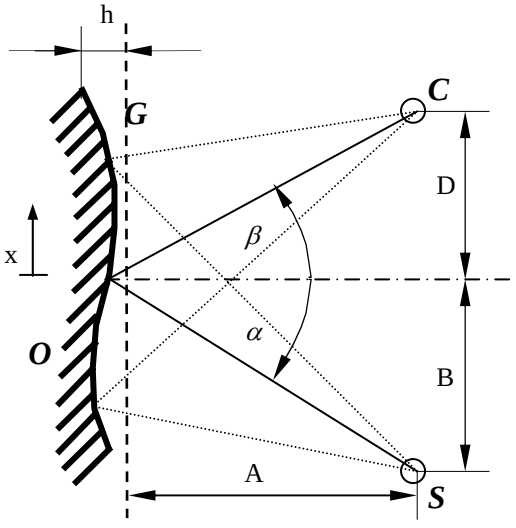

Figure 1: Shadow Moiré arrangement with constant sensitivity = tan α + tan β

Depending on the shape ***h(x,y)*** of the object surface and the angle α of illumination these shadow lines bend or distort on the surface. If a camera ***C*** observes them under an angle β through the same grating, Moiré fringes are generated that represent levels of constant depth or height of shape on the object surface. In other words, the 3D information of the object is encoded in the Moiré fringe map. Equation 1 describes the shape ***h(x,y)*** as a function of pitch ***p***, fringe order ***n***, illumination angle α and observation angle β.

$$h(x,y) = \frac{n \cdot p}{\tan\alpha + \tan\beta} = \frac{\Phi \cdot p \cdot A}{2\pi(B+D)} \tag{1}$$

However, the Moiré fringes are inherently ambiguous, i.e., if photographed only once, all sign information about the shape is lost. That is why concave and convex shapes may cause exactly the same fringe map. One convenient way to solve this sign problem for still objects is to combine Shadow Moiré with phase-shifting. Chiang, (1978) and Post et al (1989) demonstrated the feasibility of this combination by moving away either the object from the grating or vice versa. For objects as heavy as a patient, it is easier to move the grating, causing the Moiré fringes to move as well.
A phase shift of Φ = 360° is considered the exact amount of movement to replace a fringe by its neighboring one. In this study the algorithm of 4 steps was adopted, because it creates a particularly simple solution which is also fairly robust against small phase step errors. The intensities of each of the four pictures, mutually shifted by 90°, can be described as (Robinson, D. et al 1993):

$$\begin{aligned}
I_1 &= I_0 + I_m \cos(\phi) \\
I_2 &= I_0 + I_m \cos\left(\phi + \frac{\pi}{2}\right) = I_0 - I_m \sin(\phi) \\
I_3 &= I_0 + I_m \cos(\phi + \pi) = I_0 - I_m \cos(\phi) \\
I_4 &= I_0 + I_m \cos\left(\phi + \frac{3\pi}{2}\right) = I_0 + I_m \sin(\phi)
\end{aligned} \tag{2}$$

where ***I*** is the intensity captured by each pixel at the image plane of the CCD camera, I_0 is the medium intensity and I_m the modulation intensity of each pixel. Their dependency of ***x,y***-position is omitted, here, for simplicity. Solving Eq. (2) for the phase results in:

$$\phi = \arctan\left(\frac{I_4 - I_2}{I_1 - I_3}\right) \tag{3}$$

which can be computed within $-\pi \le \phi \le \pi$. The remaining 2π phase jumps can be removed by suitable algorithms of phase-unwrapping. Once the phase is obtained without phase jumps the shape ***h(x,y)*** can be calculated applying Eq. (1).

3) MATERIALS AND METHODS

In Figure 2 are shown the object surface under study. A mold of the right foot without any anomaly in relation to the studied area served as the object surface ***O***. A grating ***G*** with a pitch ***p*** = 0,8 mm was produced by printing lines on a transparency with a resolution of 720 dpi x 720 dpi which was sandwiched properly between two glass plates of 430 mm x 220 mm in order to avoid the formation of air bubbles between the plates and the transparency.

Figure 2: Plaster mold

Figure 1 shows the illumination and observation devices of the experiment. A slide projector with a 250 W lamp power was applied as a light source ***S***. A Digital Camera with a ½ inch CCD sensor, 3.207 Mega pixels resolution and a focal distance of 6 to 18 mm was used as camera ***C***.

The measurement performance depends greatly on careful alignment and the knowledge of system parameters for which the following values were determined: p = 0.80 ± 0,008) mm, A = (1000 ± 10) mm, B = (500 ± 5) mm and D = (0 ± 5) mm. The grating was mounted on a ***x-z***-guide with positioning resolution better than 10 μm. Before images were acquired, the sensitivity of the system was verified by calibrating the correct phase-step. A phase shift of 90^o was confirmed to require a 0.20 mm drive of the grating in z-direction since the system's sensitivity was unity.

After the calibration, all components of the system were fixed with exception to the moving grating. Two images, mutually shifted in x-direction by half the grating pitch, were taken at each phase step in order to average out the primary fringes from the grating and to enhance the visibility of secondary fringes, i.e. Moiré fringes that contain the information about the shape of the object.

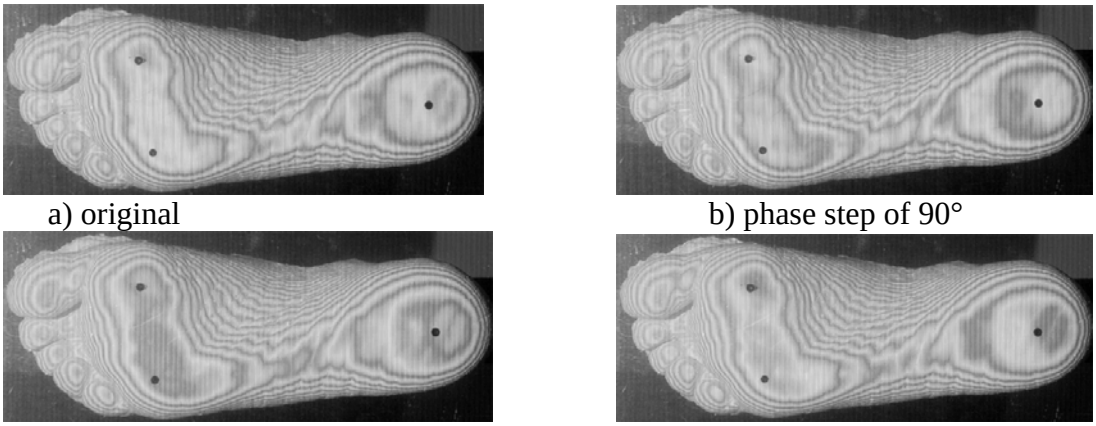

a) original b) phase step of 90°

c) phase step of 180° d) phase step of 270°

Figure 4: Average intensities as a function of phase step

The result is shown in Figure 4. These average intensities are, first, used as input to calculate the sine- and cosine-component of the phase map respectively. The remaining noise caused from the primary (grating) fringes is, then, completely removed from these components in order to smooth the phase map obtained with Eq. (2). Figure 5 gives an illustration of this filtering process.

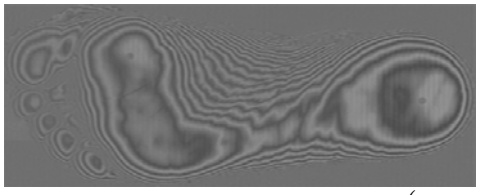

a) smoothed sine component of $\phi\ (I_4 - I_2)$

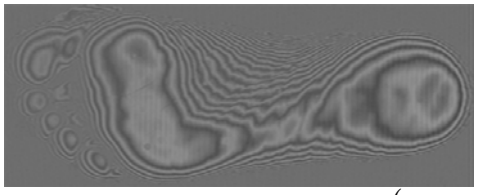

b) smoothed cosine component of $\phi\ (I_1 - I_3)$

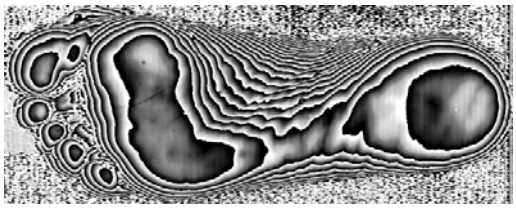

c) wrapped phase ϕ after smoothing

Figure 5: Removing residual noise from the wrapped phase map

It can be noticed in Figure 5c that a lot of phase noise is present outside the region of interest, i.e. the foot, which turns further analysis more difficult. Therefore, the modulation Intensity $\boldsymbol{I_m}$, being expressed by

$$I_m = \sqrt{\frac{1}{2} \cdot \left[(I_1 - I_3)^2 + (I_2 - I_4)^2 \right]} \qquad (4),$$

was used to test each pixel of the phase map whether it belongs, or not, to the region of interest. Only pixels that modulated above a predetermined threshold were added to the phase map for unwrapping, while all the others were left out.

Eq. (2) shows that the maximum interval of the phase calculated from the arctan function is $-\pi \le \Phi \le \pi$, for the case that the sign of nominator and denominator are considered. Thus, at each cycle of 2π corresponding to every 2 mm in the profile, a phase discontinuity is introduced into the phase map. This can be seen in Figure 5c where values of $\boldsymbol{\Phi}$ in the range of $0....2\pi$ were transformed linearly into 256 Grey levels. An abrupt transition of white to black represents a phase increase and an increasing profile, while a transition of black to white represents a decrease. Hence, the next step in the measuring process is to find the fringe orders automatically inside the region of interest in order to remove multiple phase-jumps. Figure 6a shows the fringe order map that was determined by the phase unwrapping algorithm. Once the fringe order is known Eq. (1) is used to compute the resulting profile of the foot in mm. Figures 6b shows it as a grey level picture.

a) 2D plot of fringe order map

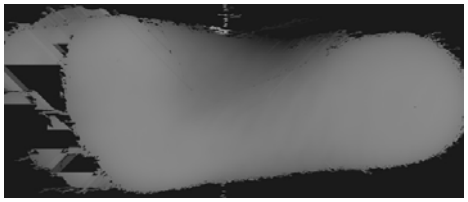

b) 2D plot of foot (*h(x,y)* in Grey level)

Figure 6: Fringe order map and 2d plot in grey level

4) ERROR ANALYSIS

In order to estimate the combined measurement error of the system described above, the Taylor expansion was applied to Eq. (1), assuming normal distribution and statistical independence of each system variable. Further, it is considered, that all uncertainties have infinite degree of freedom and a confidence interval of 95%. Then, the combined measurement uncertainty (ISO GUM 1998) can be simplified to

$$U_{95}^2(h) = \left(\left|\frac{\partial h}{\partial \phi}\right| \cdot U_{95}(\phi)\right)^2 + \left(\left|\frac{\partial h}{\partial p}\right| \cdot U_{95}(p)\right)^2 + \left(\left|\frac{\partial h}{\partial A}\right| \cdot U_{95}(A)\right)^2 + \left(\left|\frac{\partial h}{\partial B}\right| \cdot U_{95}(B)\right)^2 + \left(\left|\frac{\partial h}{\partial D}\right| \cdot U_{95}(D)\right)^2 \qquad (5).$$

After some transformation of Eq. (5) the relative uncertainties can be expressed as

$$\frac{U_{95}(h)}{h} = \left\{\left(\frac{U_{95}(\phi)}{\phi}\right)^2 + \left(\frac{U_{95}(p)}{p}\right)^2 + \left(\frac{U_{95}(A)}{A}\right)^2 + \left(\frac{U_{95}(B)}{B+D}\right)^2 + \left(\frac{U_{95}(D)}{B+D}\right)^2\right\}^{\frac{1}{2}} = 5.4\% \qquad (6).$$

Introducing the measurement results obtained for the geometric parameters ***p***, ***A***, ***B*** and ***D*** in Eq. (6) it follows that their contribution to the combined uncertainty is 1% respectively. The relative uncertainty of the phase is dominated by the phase-stepping and was estimated in the range of 1/20 of a fringe order, i.e. 5%. Eq. (6) estimates the combined uncertainty of the measurement system to 5.4%.

5) MEASUREMENT RESULTS AND COMPARASION METHODS

In order to verify the reliability of the Shadow Moiré system the profile of the plaster mold was also measured by a CNC coordinate measurement machine (CMM). A map of approximately 7600 points was obtained by the CMM with a maximum error of ± 0.01 mm. The result of this measurement is illustrated in figure 7a) as a 2D-plot and in figure 7b) as a 3D-plot. Since its uncertainties are insignificant compared to the uncertainties of Shadow Moiré, expected through equation (6), these results can be considered, here, the comparison standard.

The map of approximately 36.000 measurement points collected by the Shadow Moiré system is shown in figures 7c) an 7d). The results of both measurement methods had to be transformed into a common coordinate system prior to comparison. Finally, figures 7e) and 7f) show the difference between both measurement methods and, therefore, represent the measurement error of the Shadow Moiré system. All scales in figure 7 represent values in mm for simplification of visualization.

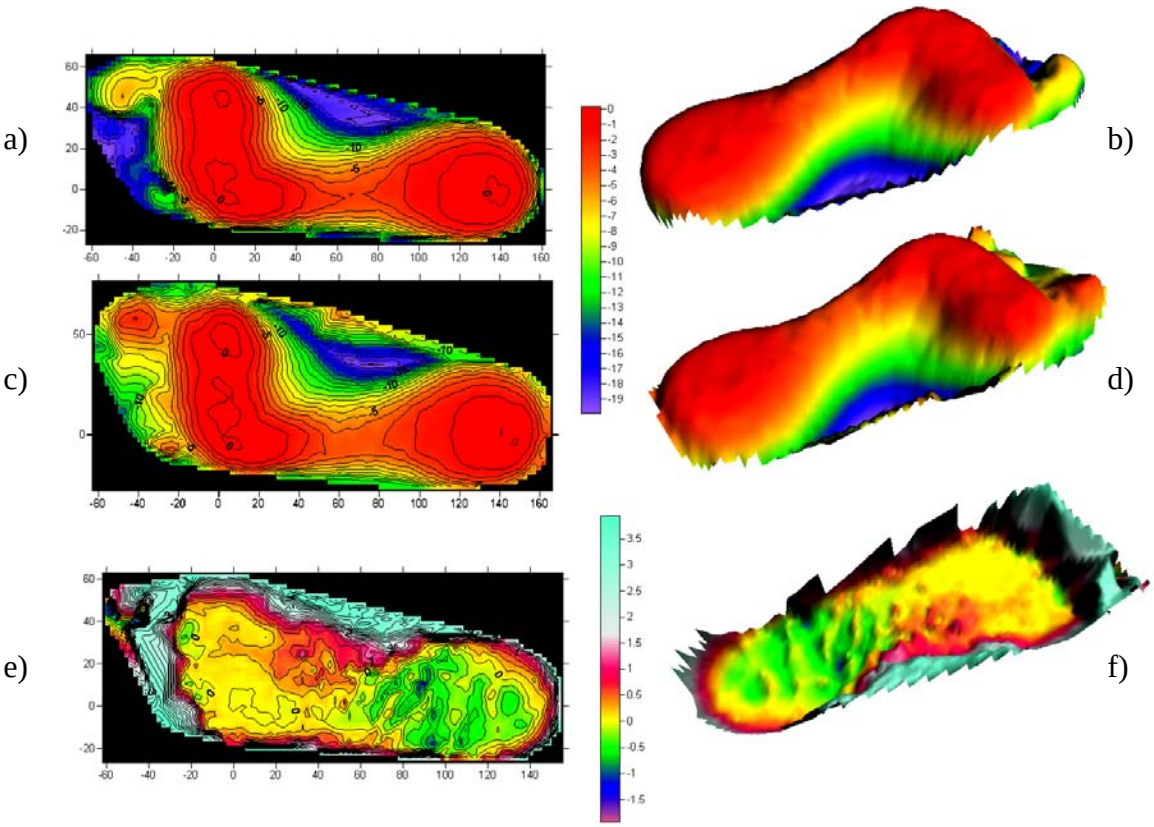

Figure 7: Comparison of Shadow Moiré with CNC coordinate measurement machine

6) DISCUSSION

The measurement results introduced into the error analysis of chapter 4 were obtained by repeated measurements, common sense and a priori information. The combined uncertainty of the order of 5% is already considered sufficiently small for most problems involving diagnoses. The uncertainty budget demonstrates that the measurement uncertainty of the whole system depends significantly upon how good phase measurements can be performed. The analysis presented so far does not include any contributions from nonlinear terms of the Moiré, nor distortions of the illuminating and imaging system. However, the previously estimated measurement uncertainty for Shadow Moiré could be confirmed by direct comparison with a CMM as standard. Some of the residual errors are most probably due to difficulties encountered matching the two point maps in one common coordinate system, rather than major errors of Shadow Moiré itself.

An enormous advantage observed with the moiré technique in relation to contact measurements is the time spent for acquisition of the point map and amount of acquired data. While the CMM usually required an average of one day to map less than 7000 points, equidistantly distributed over the plaster mold, the Shadow Moiré system needed only several minutes in order to acquire and fully process more than 36000 measurement points. It should be noted, that this time might be decreased down to several seconds, once the system is completely automated.

In the phase map one can notice areas of the plantar arch with high slope and, thus, high fringe density that show insufficient fringe contrast for quantitative evaluation. However, the amount of details measured as well as the quality of measurement data is already sufficient for means of diagnosis. The authors are currently working to implement a compact modular system for shape measurements that can be run by medical personal in private offices.

7) CONCLUSIONS

It is concluded that Shadow Moiré method combined with Phase Shifting can be used for the measurement of the medial plantar arch. The estimated measurement error of the order of 5% is more than satisfactory for applications in the area of medical engineering. However some improvements can be made in the acquisition and the processing of images. The efforts should focus, mainly, in the measurement of the phase ϕ, since it is the most significant contributor to the total uncertainty of the system. The studies undertaken can be applied to investigate other parts of the human body. Currently, the authors are adapting the system for measurements of the human back for diagnoses of congenital defects of the spine.

8) ACKNOWLEDGEMENTS

The authors gratefully thank Dr. Juan Campos Rúbio for providing the measurements using the CMM.

9) REFERENCES

Andrews J.R.; Harrelson , G.L., 2000, **"Physical Rehabilitation of the Sport Lesions"** Ed. Koogan, Rio de Janeiro, 2ª edition, pp.323-336.

Chiang, F.P., Kim, R.C., 1978, **"3D Vision System Analysis and Design"** in Three-Dimensional Machine Vision, 153p.

Gardner, W. D..; M.D., Osburn, W.A., 1974, "**Human Anatomy"**. São Paulo- SP: Publisher Atheneu.

Hanra, A & Volpon, J., 1994, **" Photopodometry Quantitative Moiré in the Evaluation of the Plantar Arch"**, USP, Ribeirão Preto.

Hebert, H & Xavier, R.,2003, **"Orthopedics and Traumatology"**.Ed. Artmed, São Paulo, 3ª edition, pp.662-671.

ISO GUM (1998)

Post, D; Han B & Ifju P., 1989, **"High Sensitivity Moiré". Experimental Analysis for Mechanics and Materials.** Mechanical Engineering Series, Ed. Springer-Verlag, Austin, Texas, pp.322-365.

Takasaki, H. 1970, **"Moiré Topography",** Applied Optics, Vol. 9, pp.1967-1472.